

## Article

# Quad Sector HMSIW Tapered Slot Antenna Array for Millimeter-Wave Applications

Iftikhar Ahmed <sup>1</sup>, Sultan Shoaib <sup>2,\*</sup>  and Raza Ali Shah <sup>1</sup>

<sup>1</sup> Department of Electrical Engineering, HITEC University, Taxila 47080, Pakistan; iftikhar.ciit@hotmail.com (I.A.); raza.ali.shah@hitecuni.edu.pk (R.A.S.)

<sup>2</sup> School of Applied Sciences, Computing and Engineering, Wrexham Glyndwr University, Mold Road, Wrexham LL11 2AW, UK

\* Correspondence: sultan.shoaib@glyndwr.ac.uk

**Abstract:** In this paper, a slot antenna array based on a half-mode substrate integrated waveguide (HMSIW) is presented, integrating a series of linearly tapered slots for wireless broadband applications in millimeter-wave frequencies. The slots are etched on the upper layer of HMSIW, which radiates the energy from the open side of HMSIW, exhibiting a near broadside radiation pattern. Two identical sets of back-to-back printed antenna arrays are cross-lap joined to form a quad sector antenna providing 360° coverage. The proposed antenna occupies a volume of 20 × 20 × 70 mm<sup>3</sup>. The measured bandwidth is 1.81 GHz (6.53%) for Voltage to Standing Wave Ratio (VSWR) 3:1 from 26.8 to 28.6 GHz, while the peak measured gain and efficiency of single antenna array were 14.2 dB and 71.3%, respectively, at 27.5 GHz. Furthermore, the sidelobe level in the azimuth plane was observed to be 17.75 dB. The performance of the proposed antenna is measured, and a good agreement between simulation and measured results is observed over the frequency range of 27.5–28.35 GHz for millimeter-wave 5G applications.



check for updates

**Citation:** Ahmed, I.; Shoaib, S.; Shah, R.A. Quad Sector HMSIW Tapered Slot Antenna Array for Millimeter-Wave Applications. *Electronics* **2021**, *10*, 1645. <https://doi.org/10.3390/electronics10141645>

Academic Editor:  
Hirokazu Kobayashi

Received: 19 February 2021  
Accepted: 7 July 2021  
Published: 10 July 2021

**Publisher's Note:** MDPI stays neutral with regard to jurisdictional claims in published maps and institutional affiliations.



**Copyright:** © 2021 by the authors. Licensee MDPI, Basel, Switzerland. This article is an open access article distributed under the terms and conditions of the Creative Commons Attribution (CC BY) license (<https://creativecommons.org/licenses/by/4.0/>).

**Keywords:** slot antenna array; half mode substrate integrated waveguide (HMSIW); substrate integrated waveguide (SIW); linearly tapered slot; 5G fixed wireless access (FWA)

## 1. Introduction

The demand for high data rates in cellular networks is manifold during the last decade. To satisfy the needs of such high data throughput, additional bandwidths are required, which is not possible in existing cellular technologies due to the overcrowded spectrum. Future broadband networks are aimed to utilize more bandwidth in the unexplored millimeter-wave spectrum resulting in a high data rate [1]. The recent development of 5G fixed wireless access (FWA) at millimeter-wave frequencies is aimed to replace the conventional fixed access broadband systems. The 5G FWA is a special case of Enhanced Mobile Broadband (eMBB), where it exploits licensed or unlicensed millimeter wave spectrum providing a competitive performance as compared to the existing cable-based broadband services [2]. The major benefits of this technology are easy and rapid deployment and low cost due to a significant reduction in the number of fiber links in contrast to existing Fiber-to-the-Home (FTTH) [3]. There are a few possible deployment strategies for FWA in 5G networks, which are wireless backhaul (WB), direct fiber (DF) and passive optical network (PON). In these backhaul transport techniques, the network architecture remains almost the same with the difference of the type of link connecting 5G access points to the network. A typical 5G FWA scenario is depicted in Figure 1, which deploys a direct fiber link from the central office to the 5G access point. The access point employs a millimeter-wave spectrum to provide network coverage to several users, and these are termed as customer premises equipment (CPE) [4]. These CPEs are crucial components in an FWA system and are categorized into outdoor and indoor CPE. The indoor CPE connects the users to the FWA network through outdoor CPE. The outdoor

CPE supports up to  $4 \times 4$  MIMO antennas offering a 10–15 dB improved signal quality as compared to an indoor CPE that supports up to  $2 \times 2$  MIMO antennas [5]. An experimental study was carried out by Ericsson to find the feasibility of a 5G FWA deployment in a suburban environment with a user density of 1000 users per square km. The minimum requirements set for each user were a data rate of 15 Mbps utilizing a channel bandwidth of 200 MHz operating on a 28 GHz band. This study assumed bidirectional data transmission using TDD duplex mode and omnidirectional antennas in indoor CPEs with a peak gain of 10 dBi. The results of this study reveal that 100% of the users had met the data rate requirement, and 93% of the users achieved a data rate of 100 Mbps [6]. The Federal Communications Commission (FCC) has auctioned various bands in the millimeter-wave frequency range including 28 GHz (27.5–28.35 GHz) as a potential candidate for providing a contiguous spectrum of 850 MHz to the high-speed data services [7]. The antenna being a core component of a wireless communication system greatly affects the system performance, and the design of antennas at such high frequencies is difficult due to the much shorter wavelength in the range of a few millimeters. The antenna systems to be used on base stations covering the complete azimuth plane are desirable. The substrate integrated waveguide (SIW) was widely used in microwave circuits and antennas. It is advantageous over the conventional rectangular waveguides (RWG) due to its low profile, low cost, ease of fabrication and integration with planar circuit components while having similar propagation characteristics [8,9]. A folded SIW (FSIW) is proposed and utilized to design waveguides and filters, which significantly reduces the size of SIW; however, the fabrication of such a multilayer structure increases the cost and complexity [10,11]. A more compact structure half-mode-integrated waveguide (HMSIW) is developed by splitting a SIW into half from the center, resulting in a magnetic wall on the open side that preserves nearly all the advantages of SIW [12]. The HMSIW is more convenient to use in space-limited applications due to its reduced size, which is merely half of a SIW, and it can support  $TE_{0,5,0}$  mode. Several studies on the antennas using the HMSIW have been presented in the literature. A HMSIW based leaky-wave antenna for the Ka-band is presented [13]. Despite having a wide bandwidth, the conical shaped quasi-omnidirectional radiation pattern limits its application to vehicular communication. Two transverse slot antenna arrays for X and Ka bands are designed by studying the field distribution and phase constant of a single slot providing a broadside radiation pattern in both bands [14]. However, the Ka-band antenna provides a narrow bandwidth of only 2.7%, and undesired grating lobes are observed in the E-plane. Several HMSIW antennas are proposed and developed which incorporate composite right/left-handed (CRLH) structures providing backward to forward and broadside radiation for the designed frequency range [15,16]. A multibeam slot antenna array is developed by utilizing SIW based hybrid couplers and a feeding network [17]. However, this SIW based longitudinal slot antenna array suffers from the large overall dimensions. The antenna proposed in [18] uses a series of antipodal linearly tapered slot radiating elements exploiting edge radiation providing forward radiation, while the antennas in [19] use a transverse slot and combination of transverse and longitudinal slots to demonstrate forward to backward capability. A HMSIW based leaky-wave antenna is proposed in [20], which uses inter-digital capacitors to realize a leaky-wave behavior. A novel method is proposed in [21] to reduce the sidelobe levels of HMSIW leaky wave antennas, and the presented antenna covers the millimeter-wave 5G frequency band from 26 to 30 GHz. A high-gain sparse phased array antenna with wide-angle frequency beam scanning capability is proposed in [22], operating at 5.8 GHz exhibiting a narrow impedance bandwidth. A leaky-wave antenna for 5G wireless devices with an operation bandwidth of 28.3–29 GHz is proposed and fabricated using low temperature co-fired ceramic (LTCC) technology that uses embedded cavities to reduce the sidelobe levels [23]. A dual beam-scanning leaky-wave antenna is proposed in [24], utilizing cascaded unit cells to cover two separate frequency bands radiating linearly polarized wave in lower band and circularly polarized waves in upper band. Table 1 provides a comparison between the antennas presented in literature and the antenna array proposed in this paper. The antennas

presented in the literature mentioned earlier utilize the HMSIW technique to reduce the overall dimensions, fabrication cost and complexity, but due to their leaky-wave nature, the drift in main lobe direction with respect frequency make these antennas suitable for frequency beam scanning applications. They lack the capability of covering a complete azimuth plane and are not suitable for such applications where  $360^\circ$  coverage is required. The antennas presented in the literature are compared with the proposed antenna for a few parameters such as operating frequency range, gain, overall dimensions of the antenna array, configuration and azimuth angle coverage. The antenna proposed in this paper is capable to cover complete azimuth plane while providing a high gain in a  $90^\circ$  sector.

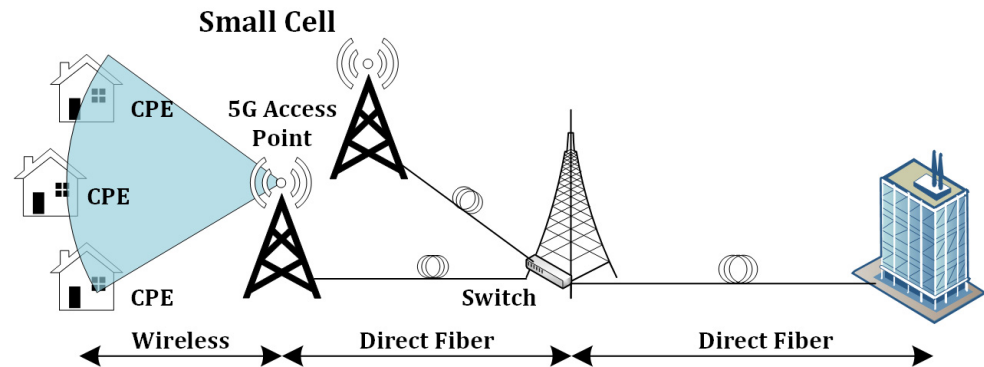


Figure 1. Fixed Wireless Access scenario with fiber backhaul.

Table 1. Comparison of similar antennas in terms of frequency, gain, antenna length,  $360^\circ$  azimuth angle coverage capability and configuration.

Ref.	Frequency Band	Gain (dB)	Antenna Length	$360^\circ$ Azimuth Angle Coverage	Configuration
This work	26.8–28.6 GHz	14.2	$6.5 \lambda$	Yes	4 Antenna Arrays
[20]	28–31 GHz	10.14	$5 \lambda$	No	1 Antenna Array
[21]	26–30 GHz	10.6	$6 \lambda$	No	1 Antenna Array
[23]	28.3–29 GHz	7.6	$4 \lambda$	No	1 Antenna Array

## 2. Design Procedure

Figure 1 describes the difference between SIW and HMSIW based transmission lines. Initially, a HMSIW based transmission line is simulated, and design parameters such as the diameter of via  $d$  and spacing between vias  $p$  are optimized to minimize the radiation leakage. A single tapered slot is introduced on the top metal surface of the HMSIW transmission line to realize a tapered slot antenna. Various design parameters are simulated, and a comprehensive parametric analysis is presented. Based on the optimized single tapered slot antenna, an array antenna is proposed to enhance the directivity of the antenna. The number of slots in the array is studied, and the effect on radiation pattern is reported. An FWA indoor CPE can have multiple sectors to improve the signal reception and system capacity. An orthogonal arrangement of four identical tapered slot antenna arrays is proposed, which enables the coverage of the complete azimuth plane while maintaining a gain above 10 dBi to satisfy the requirements of 5G FWA. A low loss microwave substrate, Rogers RT Duroid 5880, with a dielectric constant of 2.2, a thickness of 0.508 mm and a dielectric loss tangent of 0.0009, is used in this design.

### 2.1. Design of HMSIW

It was validated through simulation and experimental results that a substrate integrated rectangular waveguide (SIRW), later referred to as SIW, has similar dispersion properties as a conventional rectangular waveguide. An empirical approximation to compute the width of a SIW is described in [25] as,

$$w_{eff} = w - \frac{d^2}{0.95p} \tag{1}$$

where  $w_{eff}$ ,  $w$ ,  $d$  and  $p$  are the width of an equivalent rectangular waveguide, the width of SIW, diameter and spacing between shortening vias at the sides of SIW, respectively. A deviation from experimental results is observed for larger values of  $d$ . A more accurate empirical approximation is proposed in [26] as,

$$w_{eff} = w - 1.08 \frac{d^2}{p} + 0.1 \frac{d^2}{w} \tag{2}$$

A HMSIW can be considered half of a SIW with one side open and short-circuited vias on the other side, as can be seen in Figure 2. An equivalent model of HMSIW is proposed in [27] by considering a perfect magnetic conductor at the open side. The width of HMSIW denoted by  $W_{HMSIW}$  can be assumed as a sum of the half-width of the equivalent rectangular waveguide and an additional width  $\Delta w$  due to fringing fields at the open side.

$$w_{HMSIW} = \frac{w_{eff}}{2} + \Delta w \tag{3}$$

$$\Delta w = \left(0.05 + \frac{0.30}{\epsilon_r}\right) \times \ln \left(0.79 \frac{w_{eff}^2}{4h^3} + \frac{52w_{eff}-261}{h^2} + \frac{38}{h} + 2.77\right) \tag{4}$$

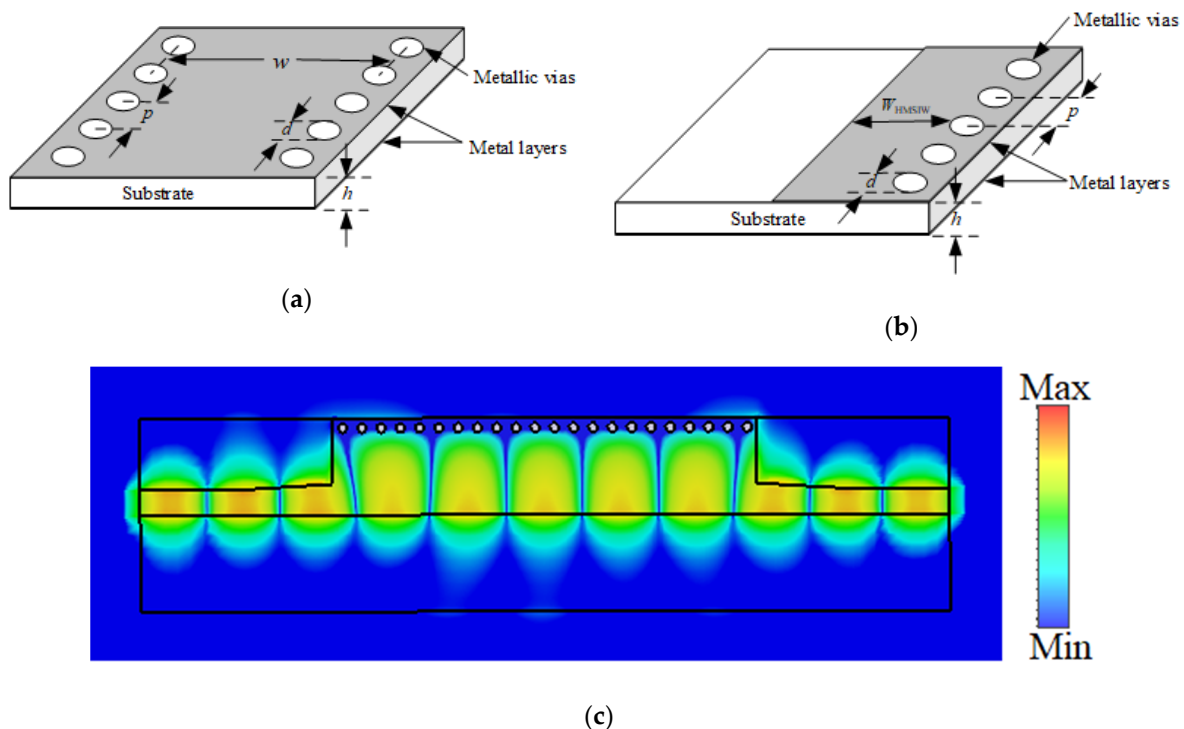


**Figure 2.** (a) Configuration of a substrate integrated waveguide (SIW); (b) Configuration of a half-mode substrate integrated waveguide (HMSIW); (c) Electric field distribution of fundamental quasi- $TE_{0,5,0}$  mode in HMSIW.

The cutoff frequency of the quasi-TE<sub>0.5,0</sub> mode in HMSIW can be calculated as

$$f_{c,TE_{0.5,0}} = \frac{c}{4\sqrt{\epsilon_r}w_{\text{HMSIW}}} \quad (5)$$

The above formulations (2) and (3) are utilized to synthesize the width of HMSIW with a particular cutoff frequency for a substrate of thickness  $h$  and relative permittivity  $\epsilon_r$ , respectively.

## 2.2. Radiation Principle of Slot Pair

The magnitude of the electric field is maximum at the edge of HMSIW near the open side, which makes it a good location to insert slots for stronger radiation. The structure of HMSIW is realized by forming a series of short-circuited vias of diameter 0.5 mm and spacing of 1 mm at one side and keeping the other side open. The top metal layer covers half of the substrate in width, and the bottom metal layer has the same width as the substrate to guarantee the direction of maximum radiation in the  $xy$ -plane. The structure of HMSIW incorporating a pair of tapered slots is depicted in Figure 2.

The corresponding electric field distribution inside the HMSIW matches the fundamental quasi-TE<sub>0.5,0</sub> mode and is found similar to half of the fundamental mode quasi-TE<sub>1,0</sub> in SIW as depicted in Figure 2c. The field components of the quasi-TE<sub>1,0</sub> mode inside the HMSIW are as follows [18]:

$$E_{y,(0.5,0)} = Ak_x \sin k_x(w-x)e^{-jk_z z} \quad (6)$$

$$H_{x,(0.5,0)} = \frac{-Ak_x k_z}{\omega\mu} \sin k_x(w-x)e^{-jk_z z} \quad (7)$$

$$H_{z,(0.5,0)} = \frac{A(\epsilon_r k_0^2 - k_z^2)}{j\omega\mu} \cos k_x(w-x)e^{-jk_z z}, 0 \leq x \leq w \quad (8)$$

where  $\omega$  and  $\mu$  are angular frequency and permeability of the material inside HMSIW. The parameters  $k_x$  and  $k_z$  are,

$$k_x = \frac{\pi}{2(w-a)} \quad (9)$$

$$k_z = \sqrt{\epsilon_r k_0^2 - \left(\frac{\pi}{2(w-a)}\right)^2} \quad (10)$$

where  $a$  is the position of the maximum electric field in the  $x$ -axis. The total field radiated can be assumed as a sum of electric fields radiated by the open side and the slot pair. The radiation field radiated by the open side can be obtained from (6), assuming the value of  $w = 0$  at the open boundary.

## 2.3. HMSIW Single Slot Antenna and in an Array Configuration

Figure 3 shows the configuration of the HMSIW slot antenna identifying all design parameters, which are given in Table 2. A linear tapered slot is introduced as the radiating element in the upper layer of HMSIW, which is fed by a microstrip feed, and a microstrip transition is used. The substrate used is Rogers RT/Duroid 5880 with a dielectric constant of 2.2 and thickness of 0.508 mm. The proposed antenna is designed in a 3D EM simulation and analysis software CST Microwave Studio. A parametric analysis is performed to observe the effect of the design parameters on the reflection coefficient.

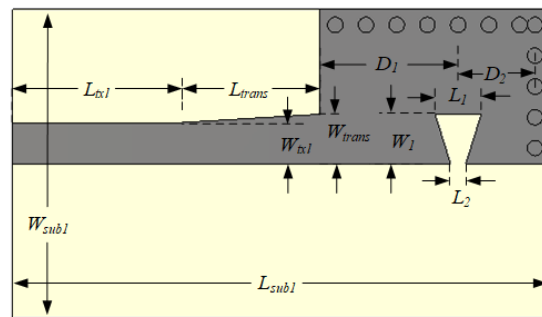


**Figure 3.** Configurations of HMSIW tapered slot antenna incorporating a single slot.

**Table 2.** List of parameters.

Parameter	Value (mm)	Parameter	Value (mm)
$W_{HMSIW}$	3.5	$d$	0.5
$P$	1	$H_{sub}$	0.508
$W_{txl}$	1.3	$L_{txl}$	5
$W_{trans}$	1.6	$L_{trans}$	5
$D_1$	4.5	$L_1$	1.5
$D_2$	2.5	$L_2$	0.5
$W_{sub1}$	9	$L_{sub1}$	17.5
$W_{sub2}$	9	$L_{sub2}$	70
$D_3$	4.5	$D_4$	5.243
$D_5$	8.02	$D_6$	9.968

The parametric analysis presented in Figures 4 and 5 is obtained from the EM simulation of a single slot antenna. Figure 4a shows the effect of change in the width of slot  $W_1$  (mm). The optimized antenna has a slot width of 3.2 mm, which is approximately equal to the half resonant waveguide wavelength. It is evident from the theory of slot antennas that the resonating frequency is inversely proportional to the width of the slot, and similar behavior is observed. The change in resonant frequency is relatively small while the length of the slot  $L_1$  (mm) is altered, which is due to the change in the impedance of the slot as in Figure 4b. The opening of the slot  $L_2$  is changed from 0.3 mm to 0.5 mm, as in Figure 4c, and it is observed that it has minimal effect on the impedance matching of the antenna; rather, it changes the resonant frequency. Identifying such parameters is beneficial in antenna designing and can help in the optimization process. The distance of the slot to the horizontal vias at the end of HMSIW, termed as matching load, greatly affects the impedance matching of the antenna, consequently deteriorating the return loss as reported in Figure 4d.

The gain of an array antenna is directly proportional to the number of radiating elements, and to increase the gain, the number of slots in an array was increased from 1 to 8. A pair of linearly tapered slots separated by a distance  $D_2$  (mm) is repeated at a distance of  $D_3$  (mm), which is the spacing between slot pairs. Increasing the number of slots from 1 to 2 lowers the resonant frequency of the antenna, which is the result of coupling between the slots. Adding one more slot pair does not change the resonant frequency, but the impedance matching is degraded. When the number of slots is increased to 8, the antenna has two resonances which result in bandwidth improvement. The effect of the number of slots on  $S_{11}$  (dB) is shown in Figure 5a. The normalized radiation patterns in the elevation plane are displayed in Figure 5b, and it is observed that increasing the number of slots decreases the beam-width of the antenna.

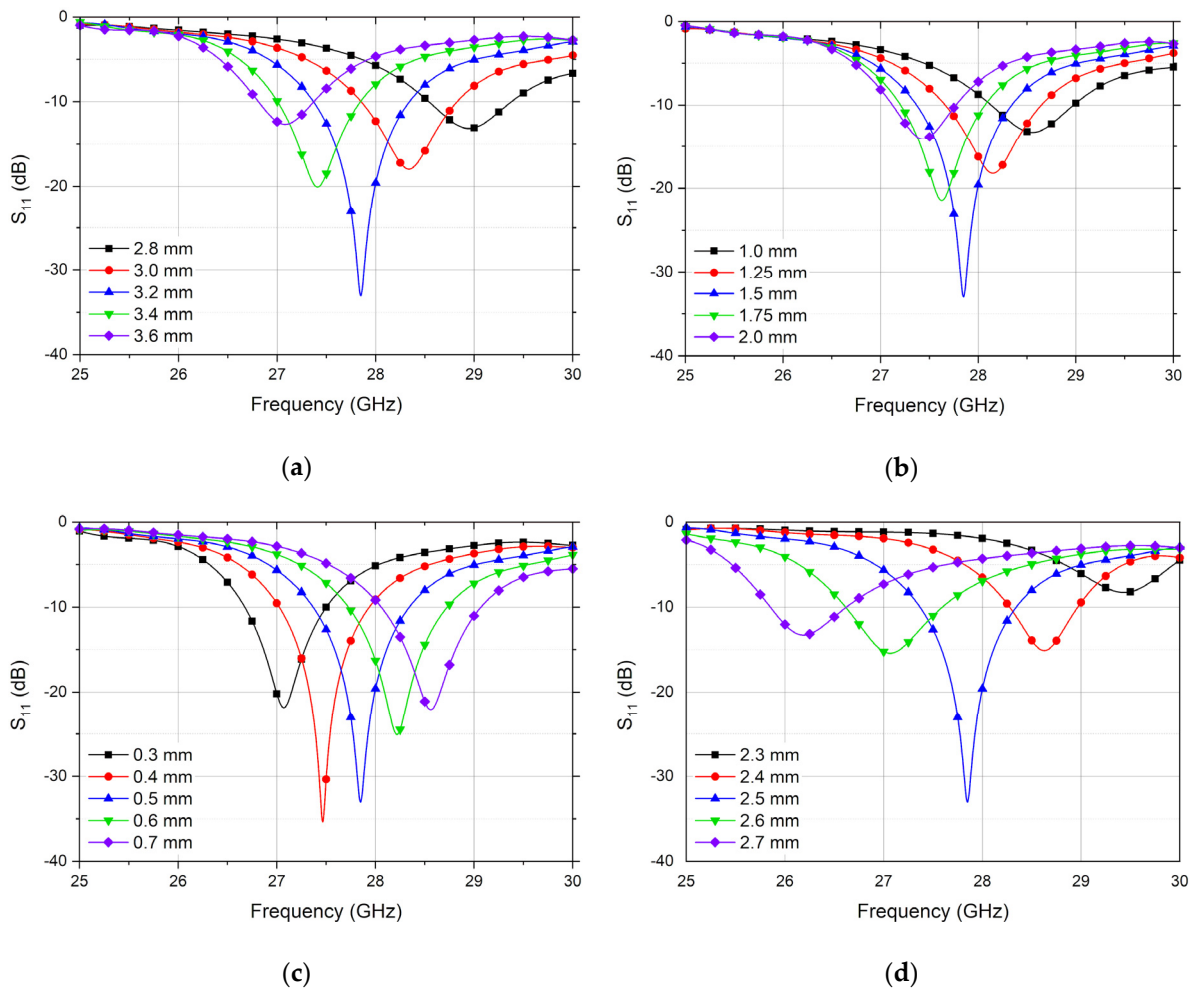


**Figure 4.** Simulated  $S_{11}$  (dB) of HMSIW single slot antenna for (a) Width of slot  $W_1$  (mm); (b) Length of slot  $L_1$  (mm); (c) Opening of the slot  $L_2$  (mm); (d) Distance of slot to the matching load  $D_2$  (mm).

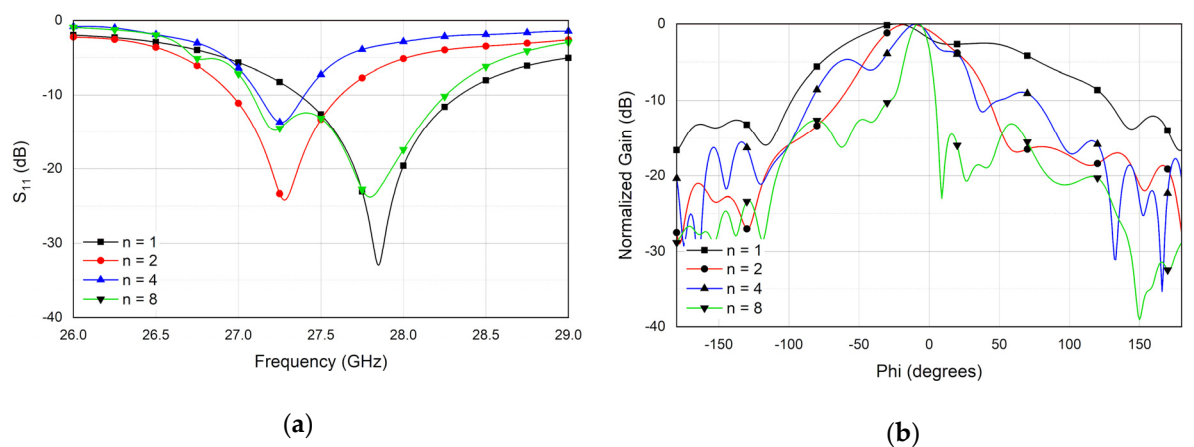


**Figure 5.** (a) Effect of number of slots on  $S_{11}$  (dB); (b) Effect of number of slots on the radiation pattern.

### 3. Quad Sector HMSIW Slot Antenna Array

The proposed antenna is fabricated using the substrate Rogers 5880 with the same electrical properties as used in the HMSIW single slot antenna. Figure 6 shows the configuration of the Quad sector HMSIW slot antenna array along with the photograph of the fabricated prototype. The structure is composed of two copies of identical HMSIW tapered

slot antenna arrays printed back-to-back on the same substrate. Two of such antenna arrays are then lap joined together to form a quad sector antenna array with an angular separation of  $90^\circ$  between adjacent antennas. The substrate and metal layers are extended by 2 mm beyond the vias opposite to the open side of HMSIW. This extended space improves the mutual coupling between adjacent antennas and reduces the complexity of the fabrication procedure. The full-wave simulation is performed using the CST Microwave Studio.

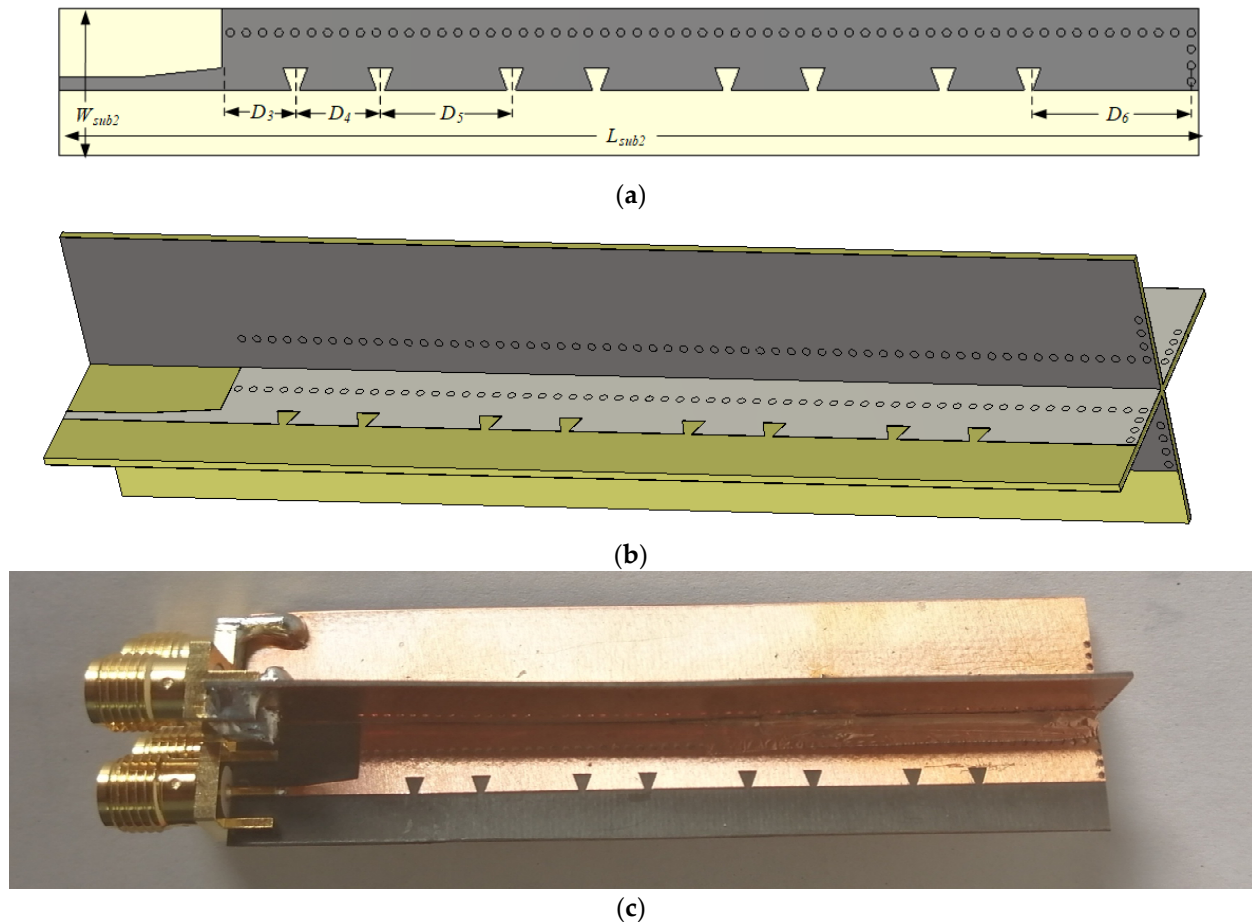


**Figure 6.** (a) Configuration of single HMSIW slot antenna array; (b) Configuration of quad sector HMSIW slot antenna array; (c) Photograph of the fabricated prototype.

### 3.1. S-Parameters

The simulated and measured results of S-parameters are shown in Figure 7. The measured results are obtained by using a Keysight Vector Network Analyzer E5080B. It can be observed that the measured reflection coefficient  $S_{11}$  (dB) is below  $-6$  dB from 26.8 GHz to 28.6 GHz, exhibiting a bandwidth of 1.8 GHz (6.53%). The isolation between antennas is observed to be less than  $-35$  dB over the desired frequency range. The difference observed between the simulated and measured results is due to the etching error and imperfect soldering of antennas.

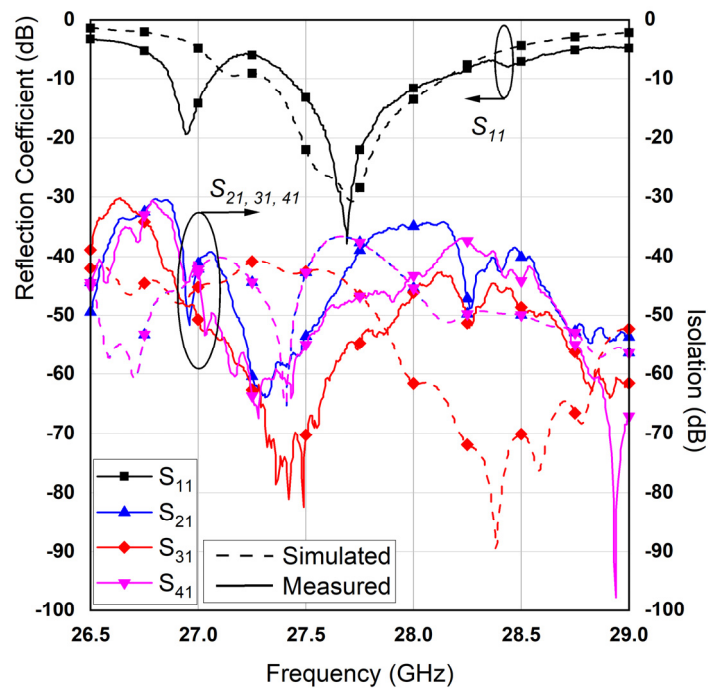


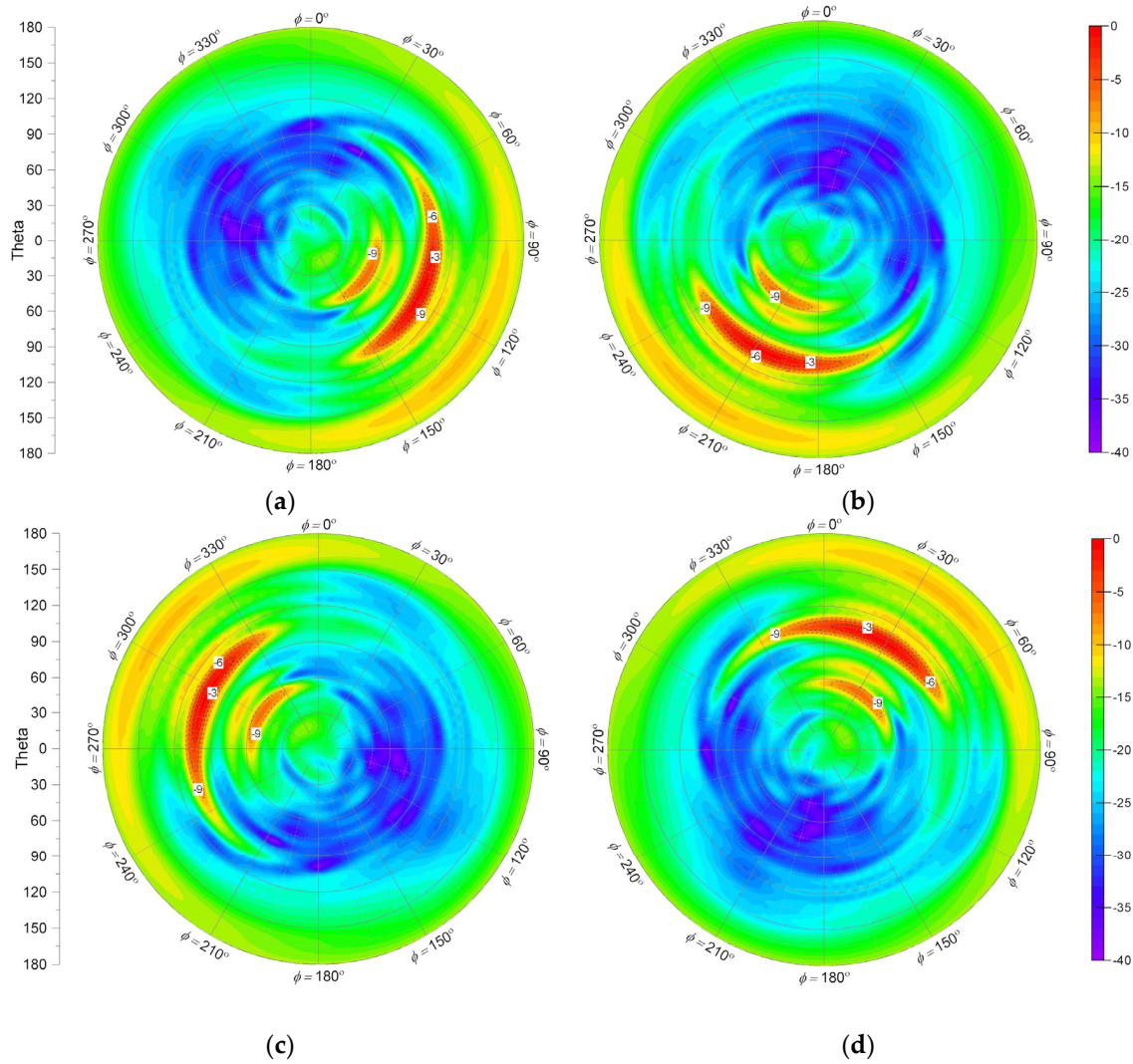
Figure 7. Measured and simulated S-parameters for the quad sector HMSIW leaky-wave antenna.

### 3.2. Radiation Performance

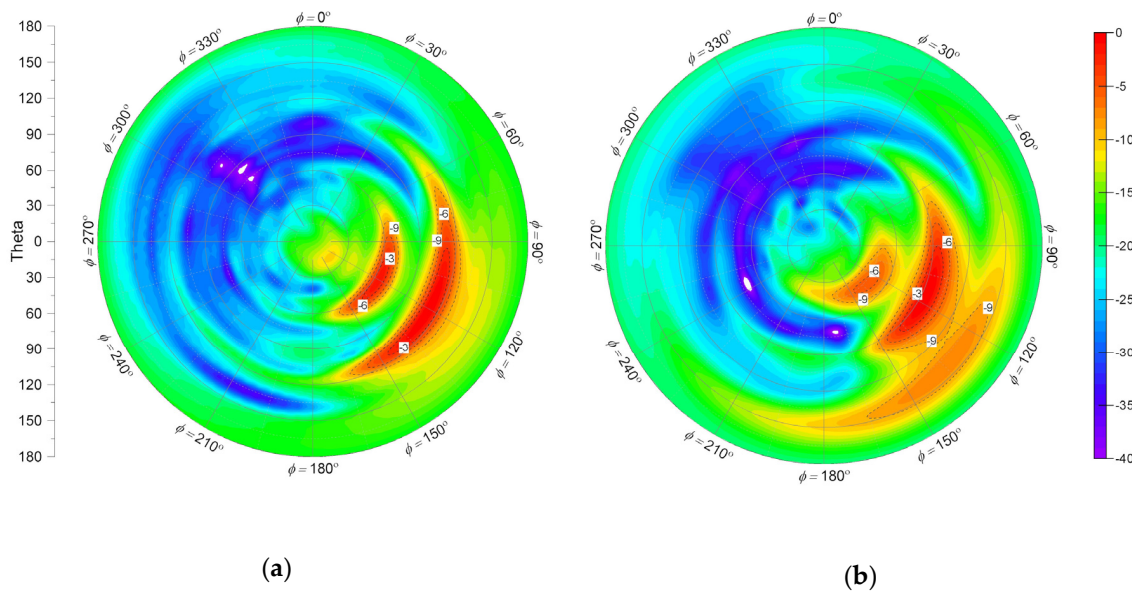
The simulated normalized 3D radiation patterns for all four antennas at 27.5 GHz are presented in Figure 8. In accordance with the configuration of the antenna, the radiation pattern is identical for all four antennas having main lobes oriented at angles  $110^\circ$ ,  $200^\circ$ ,  $290^\circ$  and  $20^\circ$  in azimuth plane and  $105^\circ$  in elevation plane for antenna 1, 2, 3 and 4, respectively. The simulated normalized 3D radiation patterns at 27 GHz, 28 GHz and 28.5 GHz are presented in Figure 9. It can be seen that the sidelobe level is below  $-17.75$  dB in the azimuth plane, and the radiation pattern is almost symmetric around the orientation of the main lobe. A comparison of the peak measured realized gain and radiation efficiency is provided in Table 3, and it is evident that these are in the range of 10–14.2 dB and 40–70%, respectively, over the frequency band 27.8–28.6 GHz.

Table 3. Measured radiation performance.

Frequency (GHz)	Sim. Gain (dB)		Meas. Gain (dB)		Sim. Efficiency (%)		Meas. Efficiency (%)	
	Ant 1/Ant 2	Ant 1/Ant 2	Ant 1/Ant 2	Ant 1/Ant 2	Ant 1/Ant 2	Ant 1/Ant 2	Ant 1/Ant 2	Ant 1/Ant 2
27	10.47/10.47	10.47/10.47	9.87/9.52	9.87/9.52	41.6/41.6	41.6/41.6	33.2/31.2	33.2/31.2
27.5	14.81/14.8	14.81/14.8	14.2/13.9	14.2/13.9	81/81	81/81	71.3/68.7	71.3/68.7
28	14.53/14.52	14.53/14.52	13.9/13.7	13.9/13.7	78.6/78.6	78.6/78.6	69.7/65.1	69.7/65.1
28.5	10.97/10.96	10.97/10.96	10.1/9.89	10.1/9.89	50.3/50.3	50.3/50.3	42.1/39.1	42.1/39.1



**Figure 8.** Simulated 3D normalized radiation patterns of the quad sector HMSIW slot antenna array at 27.5 GHz for all four antennas (a) Antenna 1; (b) Antenna 2; (c) Antenna 3 and (d) Antenna 4.



**Figure 9.** Cont.

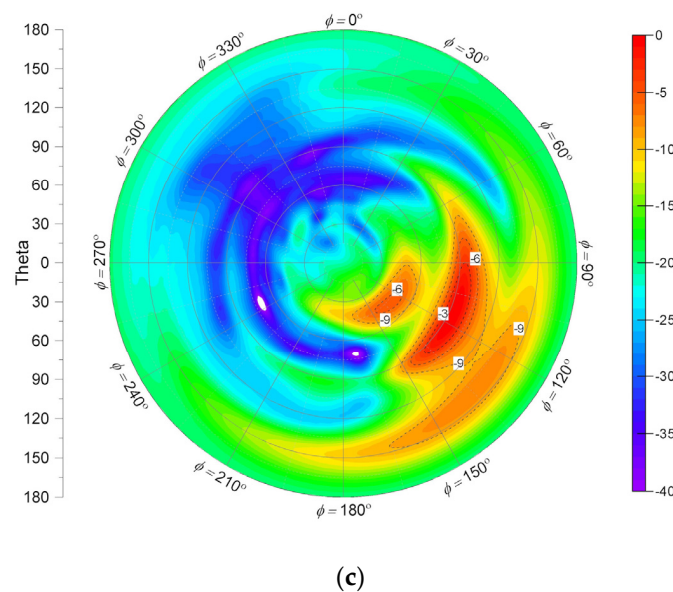


**Figure 9.** Simulated 3D normalized radiation patterns of the quad sector HMSIW slot antenna array at different frequencies (a) 27 GHz; (b) 28 GHz and (c) 28.5 GHz.

#### 4. Conclusions

A low-profile HMSIW fed tapered slot antenna array is presented in a quad sector configuration for 5G millimeter-wave access points. Full-wave analysis of the structure estimates that the resonant frequency decreases with the increase in the slot length, and it can be tuned by changing the opening of the slot. The number of slots is increased from 1 to 8 to enhance the gain of a single antenna array. A quad sector antenna system is proposed by arranging four identical HMSIW slot antenna arrays, each covering a quadrant of angular space on an azimuth plane. The far-field measurements show that the proposed antenna array has a maximum gain of 13.9 dB and radiation efficiency of 71%. Overall, the proposed quad sector antenna is demonstrated to be a good candidate for millimeter-wave wireless broadband applications.

**Author Contributions:** I.A. presented the idea, performed the experiments, and prepared the manuscript. S.S.'s contributions include prototype development and measurements. R.A.S. and S.S. contributed to reviewing and editing. All authors discussed the results and contributed to the final manuscript. All authors have read and agreed to the published version of the manuscript.

**Funding:** This research received no external funding.

**Conflicts of Interest:** The authors declare no conflict of interest.

#### References

1. Rappaport, T.S.; Sun, S.; Mayzus, R.; Zhao, H.; Azar, Y.; Wang, K.; Wong, G.N.; Schulz, J.K.; Samimi, M.; Gutierrez, F. Millimeter Wave Mobile Communications for 5G Cellular: It Will Work! *IEEE Access* **2013**, *1*, 335–349. [CrossRef]
2. International Telecommunication Union: Setting the Scene for 5G: Opportunities & Challenges. Available online: [https://www.itu.int/en/ITU-D/Documents/ITU\\_5G\\_REPORT-2018.pdf](https://www.itu.int/en/ITU-D/Documents/ITU_5G_REPORT-2018.pdf) (accessed on 12 June 2021).
3. Topyan, K.; Ulema, M. Architectural and financial considerations for deploying 5G based fixed wireless access. In Proceedings of the 2020 IEEE International Black Sea Conference on Communications and Networking (BlackSeaCom), Odessa, Ukraine, 26–29 May 2020; pp. 1–6.
4. Xie, W.; Mao, N.; Rundberget, K. Cost comparisons of backhaul transport technologies for 5G fixed wireless access. In Proceedings of the 2018 IEEE 5G World Forum (5GWF), Santa Clara, CA, USA, 9–11 July 2018; pp. 159–163.
5. Morais, D.H. *Key 5G Physical Layer Technologies: Enabling Mobile and Fixed Wireless Access*, 1st ed.; Springer International Publishing: Berlin, Germany, 2020; p. 284.

6. Laraqui, K.; Tombaz, S.; Furuskär, A.; Skubic, B.; Nazari, A.; Trojer, E. Fixed Wireless Access on a Massive Scale with 5G. Available online: <https://www.ericsson.com/en/reports-and-papers/ericsson-technology-review/articles/fixed-wireless-access-on-a-massive-scale-with-5g> (accessed on 12 June 2021).
7. FCC mmWave R&O and FNPRM. Available online: <https://mentor.ieee.org/802.18/dcn/16/18-16-0058-00-0000-fcc-mmwave-r-o-and-fnprm.pdf> (accessed on 8 March 2021).
8. Deslandes, D.; Wu, K. Integrated microstrip and rectangular waveguide in planar form. *IEEE Microw. Wirel. Compon. Lett.* **2001**, *11*, 68–70. [[CrossRef](#)]
9. Rengarajan, S.R.; Josefsson, L.G.; Elliott, R.S. Waveguide-fed slot antennas and arrays: A review. *Electromagnetics* **2007**, *19*, 3–22. [[CrossRef](#)]
10. Grigoropoulos, N.; Young, P.R. Compact folded waveguides. In Proceedings of the 34th European Microwave Conference, Amsterdam, The Netherlands, 12–14 October 2004; pp. 973–976.
11. Grigoropoulos, N.; Sanz-Izquierdo, B.; Young, P.R. Substrate integrated folded waveguides (SIFW) and filters. *IEEE Microw. Wirel. Compon. Lett.* **2005**, *15*, 829–831. [[CrossRef](#)]
12. Hong, W.; Liu, B.; Wang, Y.; Lai, Q.; Tang, H.; Yin, X.X.; Dong, Y.D.; Zhang, Y.; Wu, K. Half mode substrate integrated waveguide: A new guided wave structure for microwave and millimeter wave application. In Proceedings of the Joint 31st International Conference on Infrared Millimeter Waves and 14th International Conference on Terahertz Electronics, Shanghai, China, 18–22 September 2006; p. 219.
13. Xu, J.; Hong, W.; Tang, H.; Kuai, Z.; Wu, K. Half-Mode Substrate Integrated Waveguide (HMSIW) leaky-wave antenna for millimeter-wave applications. *IEEE Antennas Wirel. Propag. Lett.* **2008**, *7*, 85–88. [[CrossRef](#)]
14. Lai, Q.H.; Hong, W.; Kuai, Z.Q.; Zhang, Y.S.; Wu, K. Half-mode substrate integrated waveguide transverse slot array antennas. *IEEE Trans. Antennas Propag.* **2009**, *57*, 1064–1072. [[CrossRef](#)]
15. Dong, Y.; Itoh, T. Composite right/left-handed substrate integrated waveguide and half mode substrate integrated waveguide leaky-wave structures. *IEEE Trans. Antennas Propag.* **2011**, *59*, 767–775. [[CrossRef](#)]
16. Suntives, A.; Hum, S.V. A fixed-frequency beam-steerable half-mode substrate integrated waveguide leaky-wave antenna. *IEEE Trans. Antennas Propag.* **2012**, *60*, 2540–2544. [[CrossRef](#)]
17. Cheng, Y.J.; Hong, W.; Wu, K. Millimeter-wave multibeam antenna based on eight-port hybrid. *IEEE Microw. Wirel. Compon. Lett.* **2009**, *19*, 212–214. [[CrossRef](#)]
18. Henry, R.; Okoniewski, M. A broadside scanning substrate integrated waveguide periodic phase-reversal leaky-wave antenna. *IEEE Antennas Wirel. Propag. Lett.* **2016**, *15*, 602–605. [[CrossRef](#)]
19. Liu, L.; Gu, X.; Zhu, L.; Rong, Y.; Qian, H. A novel half mode substrate integrated waveguide leaky-wave antenna with continuous forward-to-backward beam scanning functionality. *Int. J. RF Microw. Comput. Aided Eng.* **2018**, *28*, e21559. [[CrossRef](#)]
20. Fu, Z.; Jiang, D.; Liu, Y. Miniaturized pattern reconfigurable HMSIW leaky wave antenna based on liquid crystal tuning technology in millimeter wave band. In Proceedings of the IEEE MTT-S International Wireless Symposium (IWS), Guangzhou, China, 19–22 May 2019; pp. 1–3.
21. Javanbakht, N.; Amaya, R.E.; Shaker, J.; Syrett, B. Side-lobe level reduction of half-mode substrate integrated waveguide leaky-wave antenna. *IEEE Trans. Antennas Propag.* **2020**, *69*, 3572–3577. [[CrossRef](#)]
22. Cheng, Y.; Ding, X.; Shao, W.; Liao, C. A high-gain sparse phased array with wide-angle scanning performance and low sidelobe levels. *IEEE Access* **2019**, *7*, 31151–31158. [[CrossRef](#)]
23. Javanbakht, N.; Amaya, R.E.; Shaker, J.; Syrett, B. A compact cavity-based leaky-wave antenna in a low temperature co-fired ceramic process with improved performance. *IEEE Access* **2021**, *9*, 25014–25024. [[CrossRef](#)]
24. Rudramuni, K.; Majumder, B.; Rajanna, P.K.T.; Kandasamy, K.; Zhang, Q. Dual-band asymmetric leaky wave antennas for circular polarization and simultaneous dual beam scanning. *IEEE Trans. Antennas Propag.* **2020**, *69*, 1843–1852. [[CrossRef](#)]
25. Cassivi, Y.; Perregrini, L.; Arcioni, P.; Bressan, M.; Wu, K.; Conciauro, G. Dispersion characteristics of substrate integrated rectangular waveguide. *IEEE Microw. Wirel. Compon. Lett.* **2002**, *12*, 333–335. [[CrossRef](#)]
26. Feng, X.; Ke, W. Guided-wave and leakage characteristics of substrate integrated waveguide. *IEEE Trans. Microw. Theory Tech.* **2005**, *53*, 66–73. [[CrossRef](#)]
27. Lai, Q.; Fumeaux, C.; Hong, W.; Vahldieck, R. Characterization of the propagation properties of the half-mode substrate integrated waveguide. *IEEE Trans. Microw. Theory Tech.* **2009**, *57*, 1996–2004. [[CrossRef](#)]